International Journal of Nanomedicine

Dovepress
Taylor & Francis Group

Open Access Full Text Article

ORIGINAL RESEARCH

# Anti-Inflammatory Combination of Puerarin and Ac2-26 Using Intranasal Delivery for Effective Against Ischemic Stroke in Rat Model

Guangzhe Xu[1], Chun Ma[2], Hongyan Chu[1], Wenxin Hu[3], Lihua Yang[2], Shuling Li[2]

[1]College of Traditional Chinese Medicine, Changchun University of Chinese Medicine, Changchun, Jilin, People's Republic of China; [2]Department of Geriatrics, Affiliated Hospital of Changchun University of Traditional Chinese Medicine, Changchun, Jilin, People's Republic of China; [3]School of Pharmaceutical Sciences, Jilin University, Changchun, Jilin, People's Republic of China

Correspondence: Lihua Yang; Shuling Li, Email ylh7239@126.com; 112338546@qq.com



**Purpose:** The pathological mechanisms underlying ischemic stroke are highly complex, with the neuroinflammatory response triggered by cerebral ischemia-reperfusion being a major contributor to secondary brain damage. This response significantly impedes neural tissue regeneration. Despite advancements in treatment, current anti-inflammatory strategies remain suboptimal in terms of safety and efficacy. This study aimed to develop an all-natural nanomedicine delivery system for the transnasal administration of puerarin, combined with the endogenous anti-inflammatory peptide Ac2-26, to enhance neuroprotection against ischemic stroke through a synergistic anti-inflammatory approach.

**Methods:** In this study, collagen nanoparticles (PueNps) loaded with puerarin were synthesized, followed by the preparation of a chitosan hydrogel. The PueNps and Ac2-26 were co-encapsulated within the hydrogel, resulting in the formation of the PueNps&Ac2-26 gel formulation. The physicochemical properties of this formulation, as well as its biodistribution and anti-ischemic efficacy in the MCAO rat brain, were evaluated.

**Results:** In this formulation system, the bioavailability of puerarin and Ac2-26 was enhanced, exhibiting sustained-release properties, which enabled efficient brain-targeted delivery. It effectively alleviated neurological impairment in MCAO rats, reduced the volume of cerebral infarction, and decreased brain water content. Additionally, the PueNps&Ac2-26 gel significantly inhibited neuroinflammation in rats and alleviated oxidative stress.

**Conclusion:** The PueNps&Ac2-26 gel is a purely natural and efficient formulation system, offering a promising approach for the clinical treatment of ischemic stroke in the future.

**Keywords:** nose-to-brain, ischemic stroke, natural nanocarrier, anti-inflammatory

## Introduction

Stroke ranks as the second leading cause of mortality among adults worldwide, with ischemic stroke accounting for 60%-70% of all cases.[1,2] Obstruction of cerebral blood flow initiates a profound inflammatory response characterized by the activation of brain-resident immune cells and infiltration of peripheral immune cells. This cascade ultimately leads to the release of proinflammatory cytokines, exacerbating brain tissue injury—a key pathological factor hindering neurological recovery after ischemic stroke.[3,4] Currently, a large number of anti-inflammatory agents have been developed preclinically to combat inflammatory damage. Still, most of them focus on the study of a single drug target, which is not only inefficient in brain targeting and makes it difficult to achieve the expected clinical efficacy but also challenging to ensure long-term safety. Therefore, there is still a need to explore safer and more effective anti-inflammatory therapies.

Puerarin, an isoflavone glycoside extracted from the Chinese herb Pueraria lobata, is a natural neuroprotective agent.[5,6] In the context of ischemic stroke, puerarin has demonstrated neuroprotective properties by mitigating inflammatory responses and alleviating oxidative stress. However, its poor solubility in both water and lipids significantly hampers absorption following oral administration, limiting its clinical utility.[7] To address these challenges, effective

Received: 7 December 2024
Accepted: 18 March 2025
Published: 25 March 2025

**Graphical Abstract**

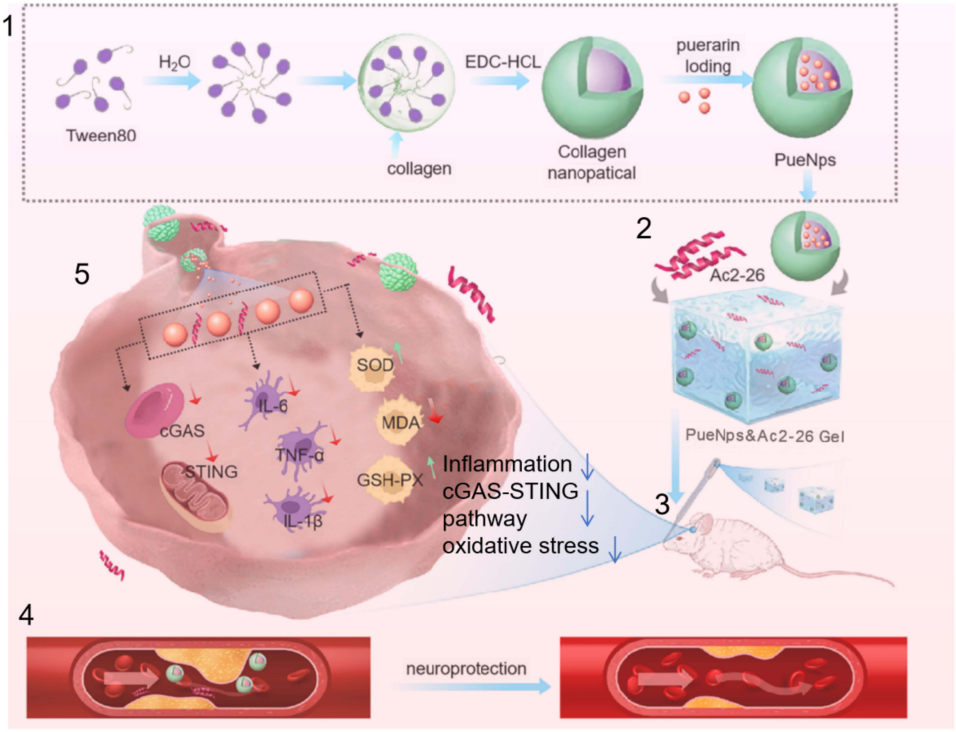


nanodrug delivery systems are required. Recently, natural biomaterials have gained attention for their potential in treating neurological diseases.[8] Among these, collagen—a natural biomedical polymer nanomaterial—has been extensively applied in clinical and drug delivery contexts due to its cost-effectiveness, accessibility, biocompatibility, biodegradability, and low immunogenicity.[9,10] Furthermore, collagen exhibits redox-active properties with some capacity for scavenging oxygen radicals.[11] In disorders such as epilepsy and focal cerebral ischemia, collagen nanoparticles have been shown to enhance drug efficacy and prolong drug action.[12,13]

However, traditional drug delivery methods face notable limitations: oral administration often results in low bioavailability and gastrointestinal side effects, while intravenous injection poses safety concerns.[14] Additionally, the blood-brain barrier (BBB) severely restricts the penetration of most drugs. Although functionalized nanomaterials have been designed to cross the BBB, their safety and efficacy remain significant challenges.[15] As a result, alternative delivery strategies are urgently needed. In this context, intranasal delivery has emerged as a promising, non-invasive approach.[16] This method bypasses the BBB, directly targeting the ischemic penumbra via olfactory, trigeminal, and cerebrospinal fluid pathways, while avoiding hepatic first-pass metabolism.[6]

Therefore, we chose intranasal delivery of puerarin-loaded collagen nanoparticles for the treatment of ischemic stroke and further optimized its efficacy. Currently, in the treatment of inflammatory diseases, supplementing endogenous pro-inflammatory resolving agents is considered a potentially superior anti-inflammatory strategy.[17] AnnexinA1 is an endogenous anti-inflammatory peptide in humans that has been exceptionally closely associated with central nervous system disorders.[18] Ac2-26, the active N-terminal peptide of AnxA1, has been shown to promote the resolution of inflammation in ischemic stroke and exhibits minimal side effects in treatment.[19,20] However, this low molecular weight anti-inflammatory peptide is highly insoluble in water and is rapidly cleared in plasma, requiring frequent administration for efficacy.[21,22] Conventional nanocarriers loaded with this relatively high molecular weight peptide result in a particle size that is too large for intranasal delivery. Therefore, for intranasal delivery of Ac2-26, hydrogel formulations are an ideal choice.

Chitosan hydrogels have the capacity to transiently open tight junctions in nasal epithelial cells and extend drug retention time in the nasal cavity under acidic pH conditions.[23,24] Our prior studies confirmed that intranasal administration of chitosan hydrogels enables sustained drug release and enhanced brain accumulation.[25] Moreover, co-loading puerarin-loaded collagen nanoparticles (PueNPs) with Ac2-26 into chitosan hydrogels effectively addresses issues related to nasal ciliary clearance and mucosal barriers.[26]

The cGAS-STING pathway plays a crucial role in the innate immune system. [27] Recent studies have demonstrated a close relationship between cGAS-STING and neuroinflammation. [28–30] In the treatment of ischemic stroke, inhibition of the cGAS-STING signaling pathway effectively suppresses the post-stroke neuroinflammatory response, reduces neuronal damage, and promotes long-term neurological recovery, making it a key and promising therapeutic approach. [31–35]

In this study, we developed a natural drug delivery system by preparing collagen nanoparticles to encapsulate puerarin, and co-loading PueNps with Ac2-26 into a chitosan hydrogel. Through nasal-to-brain delivery, we achieved the simultaneous delivery of chemical and biological agents across different drug types. This system integrates several advantages, including natural safety, non-toxicity, sustained and slow drug release, synergistic anti-inflammatory effects, and the ability to alleviate oxidative stress. The cGAS-STING signaling pathway is identified as a potential molecular target of action. Our findings lay the groundwork for a promising platform for the clinical synergistic application of novel natural drugs.

## Materials and Methods

Beef Achilles tendon purchased from Changchun Haoyue Halal Meat Industry Co (Changchun, Jilin,China).Puerarin (purity >98%) was purchased from Shanghai Yuanye Biotechnology Co (Shanghai, China). Tween 80 was obtained from Sinopharm Chemical Reagent Co (Shanghai, China). Chitosan (deacetylation degree 95%, viscosity 100–200 mPas) was purchased from Shanghai McLean Biochemical Co (Shanghai, China). 1-Ethyl-(3-dimethylaminopropyl) carbodiimide hydrochloride (EDC-HCL) was sourced from Beijing Huamaike Biotechnology Co. (Beijing, China). Acetic acid was obtained from Shanghai Aladdin Biochemical Technology Co (Shanghai, China). Sodium carbonate, disodium phosphate, and pepsin were purchased from Shanghai McLean Biochemical Co (Shanghai, China). Pentobarbital sodium, 2,3,5-triphenyl tetrazolium chloride (TTC), and hematoxylin and eosin (HE) were acquired from Sigma (St. Louis, MO, USA). All chemical reagents used in these experiments were of analytical grade, unless otherwise stated.

### Extraction and Examination of Collagen

The bovine Achilles tendon was thoroughly washed, and its fascia was removed. The tissue was then frozen and sliced into 2-mm thick slices. Sodium carbonate and disodium hydrogen phosphate were used to remove fat and heteroproteins, respectively. Collagen was subsequently extracted from the pretreated bovine Achilles tendon using a combination of acetic acid and pepsin, followed by purification through repeated salting-out and dialysis. The resulting collagen was freeze-dried to produce type I collagen sponge. Characterization of the extracted collagen was performed using sodium dodecyl sulfate-polyacrylamide gel electrophoresis (SDS-PAGE; JY-SPCT, Beijing, China) and scanning electron microscopy (SEM; JSM-IT500A, JEOL, Japan).

### Preparation of Puerarin-Loaded Collagen Nanoparticles

Puerarin-loaded collagen nanoparticles were prepared using a previously published method with minor modifications.[36] Briefly, an appropriate amount of Tween 80 was dissolved in pure water with continuous stirring until completely dissolved. Another 10 mg of collagen was dissolved in a 0.1 M acetic acid solution to obtain a concentration of 1 mg/mL. After centrifugation at 4°C and 8000 rpm for 20 minutes, 2 mL of the supernatant was added to the aqueous Tween 80 solution with continuous stirring. Collagen nanoparticles were prepared by adding 4 mg of EDC·HCl cross-linker and stirring overnight. For drug loading, puerarin was dissolved in DMSO (2 mg/mL) and added to the collagen nanoparticles, followed by continuous vortexing and ultrasonication. The hydrophobic puerarin was incorporated into the core of the collagen nanoparticles. Finally, residual EDC·HCl and DMSO were removed by dialysis (cut-off value of 12 kDa), and the nanoparticles were lyophilized and stored at 4°C for long-term stability.

## Characterization of PueNps

Transmission electron microscopy (TEM, Tecnai Spirit BioTwin, Japan) was employed to analyze the morphology of the nanoparticles. The hydrodynamic diameter (DLS) and zeta potential were determined using a dynamic light scattering particle analyzer (Zetasizer Nano ZS; UK). Fourier-transform infrared spectroscopy (FTIR; Nicolet iS10, USA) was used to detect changes in the functional groups of the collagen nanoparticles.

### Encapsulation Rate

To determine the encapsulation efficiency, puerarin-loaded collagen nanoparticles were centrifuged at 4°C, at 20,000 rpm for 30 minutes. The supernatant was collected, and the absorbance at 250 nm was measured using a UV/visible spectrophotometer. The amount of free puerarin was calculated using a standard curve, and the encapsulation efficiency was calculated using the following formula:

$$\mathrm{EE}\,(\%) = (\text{total dosage of Puerarin} - \text{free Puerarin amount})/(\text{total dosage of Puerarin})$$

$$\mathrm{LE}\,(\%) = (\text{total dosage of Puerarin} - \text{free Puerarin amount})/(\text{weight of puerarin} - \text{loaded nanoparticles})$$

### Preparation of Hydrogels

Deacetylated chitosan (4.5% w/v) was dissolved in 2 mL of 1% acetic acid and stirred continuously at 4°C until completely dissolved. Puerarin nanoparticles (PueNps) and Ac2-26, dissolved in DMSO, were slowly added to the chitosan solution. The mixture was stirred thoroughly to ensure a uniform distribution. β-Glycerophosphate (β-GP) solution (12% w/v) was added dropwise, and the mixture was stirred for an additional 30 minutes at room temperature to form the hydrogel.

### Assessment of Hydrogels

The structural morphology of the hydrogels was observed using scanning electron microscopy (SEM). Gelation time was determined using the rod-stopping method. Briefly, 5 mL of the hydrogel preparation was placed in a 20 mL beaker on a heated magnetic stirrer (Li Chen Ke Yi, Shanghai, China) and stirred at 30 rpm at 34°C. The gelation time was recorded when the magnetic bar stopped moving due to gelation. The experiment was performed in triplicate, and the average gelation time was calculated.

### Release of Puerarin and Ac2-26

For in vitro release studies, PueNps and PueNps & Ac2-26 hydrogel were each dissolved in 1 mL of distilled water and placed in dialysis bags (MWCO = 8–14 kDa). The bags were immersed in 100 mL of phosphate-buffered saline (PBS, pH 7.4) containing 1% Tween 80 at 37°C. Samples were collected at 0.5, 1, 2, 4, 8, 12, 24, 36, and 48 hours, with fresh PBS added at each sampling point to maintain the volume. The absorbance of puerarin was measured at 250 nm, and that of Ac2-26 at 210 nm using a UV/Vis spectrophotometer. Release profiles were determined by comparing the absorbance values with standard calibration curves.

## Formulation Distribution

Fluorescence distribution of the formulations was tracked in the rat brain using DiR-labeled preparations (NPs group, gel group, and combined NPs + gel group). After 0.5 and 2 hours of intranasal administration, the rats were sacrificed, and their brains were quickly removed and sectioned into regions, including the olfactory bulb, cortex, striatum, midbrain, hippocampus, cerebellum, and brainstem. The regions were homogenized, and fluorescence intensity was measured at 750/780 nm (excitation/emission wavelengths) using a plate spectrophotometer. Fluorescence intensity was converted to DiR concentration for analysis.

## Grouping of Experimental Animals and Drug Management

The experimental animals were male Sprague Dawley (SD) rats (280–320 g) purchased from Liaoning Changsheng Biotechnology Co. Ltd (Laboratory Animal Production License No. SCXK 2020–0001). All experimental animals were approved by the Experimental Animal Ethics Committee of the School of Pharmacy, Jilin University, and implemented in

accordance with the rules of implementation of the Animal Ethics Committee of Jilin University. Relevant standards are available at http://sydw.jlu.edu.cn/fgbz1/gjbz.htm.

Grouping: rats were randomly divided into 6 groups: sham operation group, MCAO model group, puerarin nanoparticles group (PueNps group), puerarin nanoparticles hydrogel group (PueNps gel group), puerarin nanoparticles and Ac2-26 hydrogel group (PueNps&Ac2-26 gel group), and i.v. injection group (PueNps&Ac2-26 gel group).

Drug management: For each group, intranasal drops were administered once daily, beginning 0.5 hours after surgery. Puerarin was administered at 0.5 mg/kg, and Ac2-26 at 0.1 mg/kg. The equivalent intravenous dose was calculated for the IV group, with an equal volume of saline administered to the model and control groups over a period of 3 days.

## The in vivo Studies Using Animal Model

A rat model of focal cerebral ischemia (MCAO) was established using the modified thread occlusion method. Rats were anesthetized by intraperitoneal injection of 3% sodium pentobarbital. After 10 minutes, the rats were fixed in a supine position on the operating table, and the anterior neck region was shaved and disinfected. The common carotid artery, external carotid artery, and internal carotid artery were exposed. A nylon thread was inserted through the external carotid artery into the internal carotid artery, and the position was marked. The thread was secured, and the incision was sutured. After 150 minutes of ischemia, the nylon thread was removed to allow reperfusion. The rats were euthanized with carbon monoxide after 3 days, and brain tissue was quickly isolated for further analysis.

## Cerebral Infarct Volume in Rats

The volume of cerebral infarction was measured using TTC staining. Following euthanasia, brain tissue was rapidly removed, frozen at −20°C for 10 minutes, and sliced into 3-mm coronal sections. The sections were stained in a 1% TTC solution at 37°C for 20 minutes, with gentle inversion every 5 minutes to ensure uniform staining. After staining, the sections were fixed overnight in 10% paraformaldehyde, photographed, and analyzed using ImageJ software (NIH, USA).

## Neurological Function Assessment and Behavioral Tests

Neurological function was assessed using the Zea Longa score (0–4 scale), mNSS score (0–18 scale), cornering test, wire-hanging test, and balance beam test.

### Turning Angle Test

Rats were placed at the center of two plates (30 cm × 20 cm × 1 cm), connected at a 30° angle. The rats were given a constant stimulus, causing them to turn toward the open end. The turning rate was recorded over 10 runs per rat. All rats were trained for 3 days prior to MCAO modeling.[37]

### Wire-Hanging Test Experiment

The wire-hanging test assessed limb grasping ability. Rats were placed on top of a wire mesh and allowed to grip the wires with all four limbs. The lid was quickly flipped over, and the time each rat remained suspended was recorded.[38]

### Balance Beam Test

Rats were placed on a balance beam, with a sponge placed beneath to prevent injury in case of a fall. The time taken by each rat to traverse the beam was recorded, with a maximum time of 120 seconds.

## Measurement of Brain Edema Content

The water content of rat brain was measured using the dry and wet weight method.[39] After euthanasia, the olfactory bulb, cerebellum, and lower brainstem were excised. The wet weight was measured immediately. The tissues were then placed in a 110°C oven for 24 hours to determine the dry weight. Brain water content was calculated using the following formula: Brain water content = (Wet weight − Dry weight) / Wet weight × 100%.

## HE Staining

Hematoxylin and eosin (HE) staining was used to observe the morphological structures of brain tissue. Sections (5 μm thick) were deparaffinized in xylene and rehydrated with ethanol. The sections were stained with hematoxylin, differentiated with ethanol hydrochloride, rinsed with tap water, and stained with eosin. The slices were dehydrated in graded ethanol, mounted using xylene, and observed under a light microscope.

## Molecular Docking

Molecular docking of puerarin (PubChem CID: 5281807) with CGAS (UniProt ID: A0A0G2JVC4) and STING (UniProt ID: F1M391) proteins was performed using AutoDock Vina 1.1.2 software. The results were visualized using PyMOL 2.4. Alphafold2 was used to model the Ac2-26 peptide, and HawkDOCK Server was employed for molecular docking of the peptide to the proteins.

## IHC

IHC was performed to detect the expression of target proteins. Dewaxed sections were incubated with 3% hydrogen peroxide for 15 minutes at room temperature and washed with PBS. Blocking was performed with 3% BSA for 30 minutes at room temperature. The sections were then incubated overnight at 4°C with primary antibodies against cGAS and STING (Beyotime, China). After washing with PBS, the sections were incubated with HRP-labeled goat anti-rabbit secondary antibody (Abcam, UK) for 40 minutes at 37°C. The sections were stained with DAB and Harris hematoxylin, and then observed under a light microscope. Images were analyzed using ImageJ software.

## Western Blot

To assess the expression of target proteins cGAS and TING, brain ischemic tissues from rats were lysed using RIPA lysis buffer. Protein separation was performed using SDS-PAGE, followed by transfer onto a PVDF membrane. The membrane was blocked with 5% non-fat milk for 1 hour, after which the primary antibody was applied and incubated overnight at 4°C. Subsequently, the membrane was incubated with HRP-conjugated secondary antibody for 1 hour at room temperature. The grayscale values were analyzed using ImageJ software.

## Enzyme-Linked Immunosorbent Assay (ELISA)

This study aimed to detect the expression of inflammatory factors and oxidative stress markers in rat brain tissue. An enzyme-linked immunosorbent assay (ELISA) kit (Shanghai Yase Biomedical Technology Co., Ltd.) was used to detect the levels of IL-1β, IL-6, TNF-α, SOD, GSH-PX, and MDA in rat brain tissues. The standard curve was established by following the instructions of each factor kit. The absorbance values of the samples at the corresponding peaks were measured using an enzyme counter, and the results were recorded and calculated.

## Cell Culture

BV2 microglial cells (Donated by the School of Life Sciences, Jilin University) were cultured in DMEM (Biosharp, Beijing, China) supplemented with 10% fetal bovine serum (FBS) (Macklin, Shanghai, China), penicillin (100 U mL−1), and streptomycin (100 μg mL−1), and incubated in a humidified environment at 37°C with 5% CO2.

## Oxygen–Glucose Deprivation/Reoxygenation Test

BV2 cells were cultured in glucose-free DMEM without FBS and exposed to a hypoxic environment with 5% CO2 and 95% N2 for 4 hours to establish the OGD model. Afterward, the culture medium was replaced with normal DMEM, and the cells were incubated under standard conditions for 24 hours. The cultured cells were divided into four groups: Control (BV2 cells without OGD injury), OGD/R, PueNps, and PueNps&Ac2-26 groups. The expression of IL-1β, IL-6, and TNF-α in the supernatants of treated BV2 cells was measured using ELISA kits according to the manufacturer's instructions.

## Statistical Analysis

All data were expressed as mean and standard deviation (mean ± standard deviation). One-way analysis of variance (ANOVA) method was performed using GraphPad Prism 8.3.0 software, and Tukey's test was repeated. p < 0 0.05 indicates a significant difference.

# Results

## Characterization of Collagen Nanoparticles

Collagen nanoparticles were successfully synthesized and characterized. Collagen, a hydrophobic protein, exhibited a fiber-like morphology, as observed by scanning electron microscopy (SEM) (Figure 1A). The nanoparticles form a hydrophobic core, promoting the loading of puerarin through hydrophobic interactions, thereby enhancing its solubility. The process flow for the synthesis of collagen nanoparticles is depicted in (Figure 1B). Dynamic light scattering (DLS) analysis showed that the hydrodynamic diameter of blank collagen nanoparticles was 122.83 ± 7.94 nm. The puerarin-loaded nanoparticles (PueNps) had a slightly larger diameter of 132.92 ± 8.44 nm, suggesting that the loading of puerarin slightly increased the nanoparticle size (Figure 1C).The polydispersity index (PDI) of the blank nanoparticles was 0.35 ± 0.04, and that of PueNps was 0.38 ± 0.05. The zeta potential of the blank nanoparticles was −25.5 ± 2.55 mV, and that of PueNps was −20.23 ± 3.26 mV, indicating that encapsulating puerarin did not significantly affect nanoparticle stability (Figure 1D and E). The encapsulation efficiency was 67.4 ± 3.2%, with a drug loading capacity of 2.68 ± 0.68%.

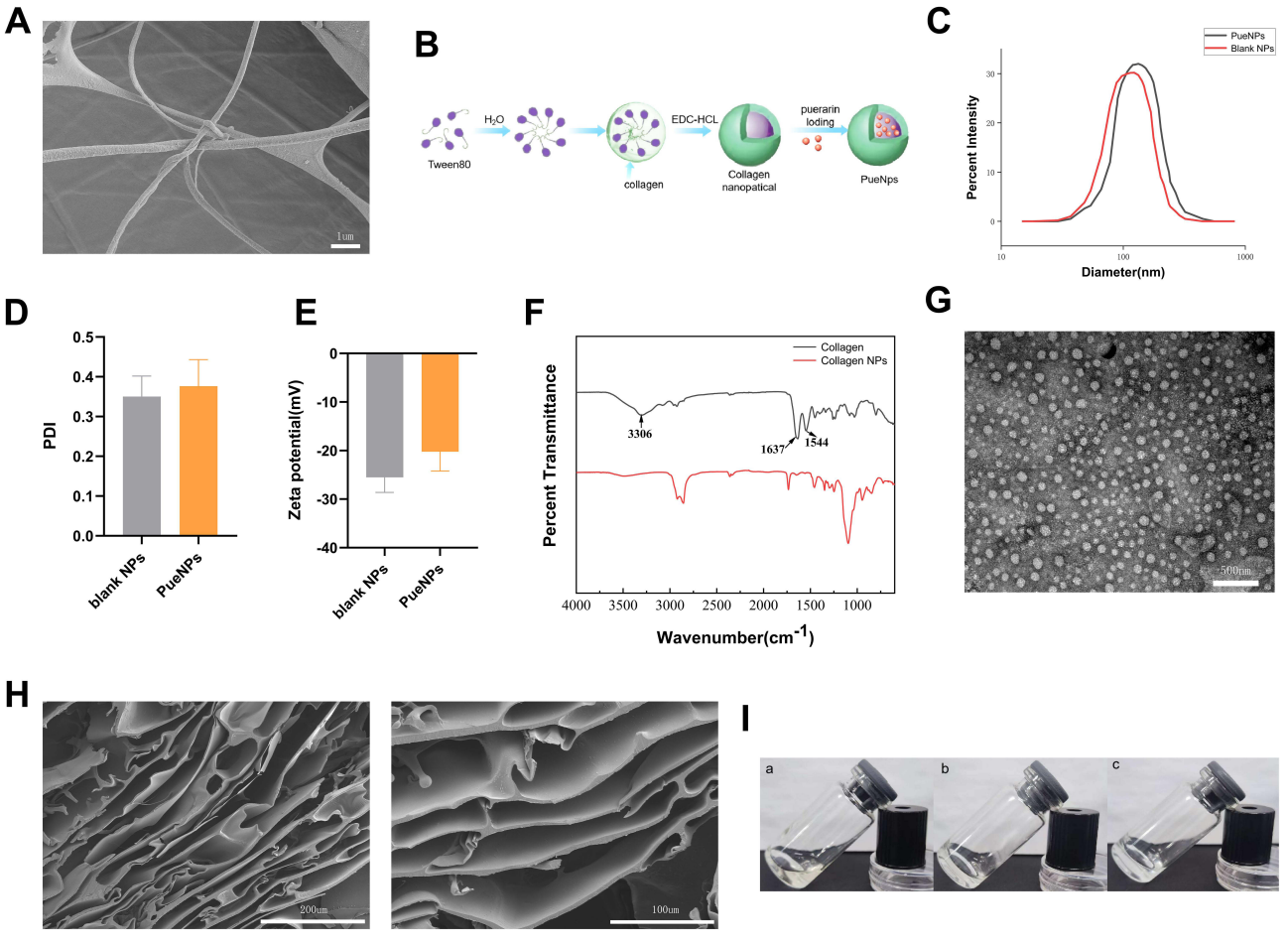


**Figure 1** Characterization of nanoparticles and hydrogels. (**A**) SEM image of collagen. Scale bar = 1 um. (**B**) Flow chart of the synthesis process of Pue-loaded collagen nanoparticles. (**C**) Particle size distribution of blank NPs and PueNPs evaluated by DLS. (**D**) PDI of blank NPs and PueNPs. (**E**) Zeta potential of blank NPs and PueNPs. (**F**) FTIR-visible absorption spectra of collagen and collagen nanoparticles. (**G**) TEM images of nanoparticles. Scale bar = 500 nm. (**H**) SEM image of the hydrogel. Scale bar = 200 um, 100 um, respectively. (**I**) Room temperature (a) vs 34 °C (b) Chitosan hydrogel state, (c) 34 °C drug-loaded hydrogel state. Data are expressed as mean ± standard deviation. (n=3).


https://doi.org/10.2147/IJN.S508800

Transmission electron microscopy (TEM) images revealed a spherical morphology of the nanoparticles (Figure 1G). Fourier-transform infrared (FTIR) spectroscopy analysis showed that, compared to pure collagen, the -NH bending peak disappeared, while the carbonyl (C=O) stretching peak was retained but slightly shifted and diminished in intensity. These changes indicate that crosslinking during nanoparticle formation altered the functional groups, with additional amide bonds formed, contributing to nanoparticle stability (Figure 1F). The stability of the nanoparticles was further confirmed by the lack of significant changes in particle size after 60 days of storage at 4°C (Supplementary Figure S1B).

## Characterization of Hydrogels

We successfully developed temperature-sensitive hydrogels by incorporating PueNps and Ac2-26 peptides into a chitosan and sodium β-glycerophosphate matrix. Vial inversion experiments demonstrated a transition from sol to gel state, confirming the temperature-sensitive properties of the hydrogel. At room temperature, the hydrogels appeared slightly pale yellow. Upon phase transition at 34°C, the gels turned white, and the addition of the drug slightly increased their transparency, though the change was not visually noticeable. No significant liquid flow was observed in the hydrogels at 34°C (Figure 1I). The gelation time was 183.8 ± 11.6 seconds, making these hydrogels suitable for intranasal administration. SEM images revealed a large surface pore structure, which facilitates the loading of nanoparticles and protein peptides (Figure 1H).

## In vitro Release

Generally, drug release can occur in various forms, such as sustained, burst, triggered, and targeted.[40] The drug release profile of the formulations is illustrated in (Figure 2A). The cumulative release of puerarin nanoparticles (PueNps) over

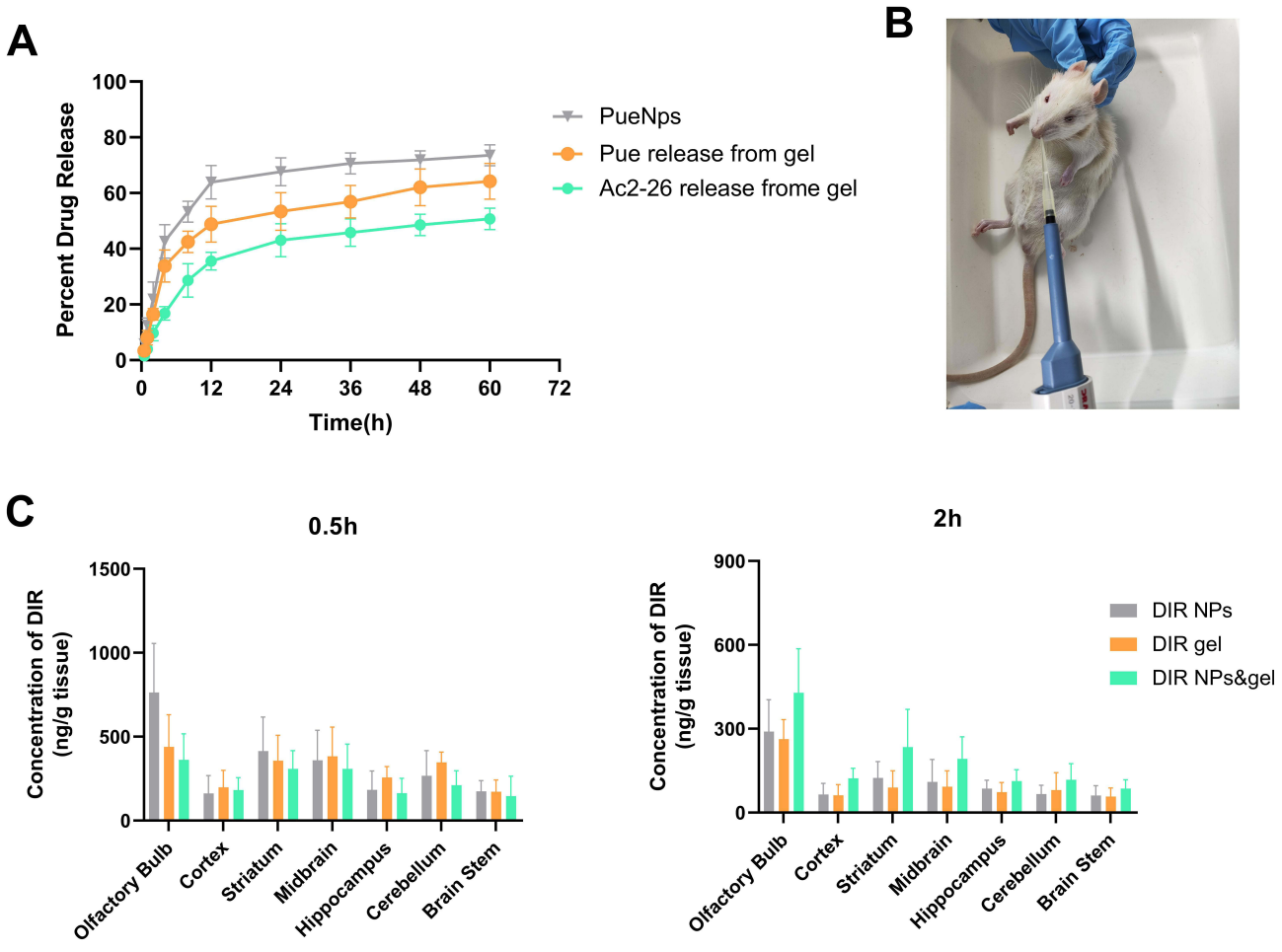


**Figure 2** Drug release and formulation distribution. (**A**) Cumulative release profiles of Pue in PueNps, Pue & Ac2-26 in PueNps & Ac2-26 gel measured over 48 hours. (**B**) Schematic of transnasal administration in rats. (**C**) Biodistribution of DIR-labeled different formulations in different brain regions in 0.5h 2h. Data are expressed as mean ± standard deviation. (n=3).

48 hours was 71.88%, as calculated from the standard curve (Supplementary Figure S1D and E). In contrast, in the hydrogel formulation, the cumulative release of puerarin and Ac2-26 was 62.02% and 48.51%, respectively, indicating that the chitosan hydrogel effectively retarded puerarin release, with Ac2-26 release being even slower. These results suggest that the nanoformulation system demonstrates slow-release properties.

## Formulation Distribution

Intranasal delivery of the formulations resulted in drug distribution across various regions of the brain, including the olfactory bulb, striatum, and midbrain, as shown in (Figure 2B). The drug entered the brain via multiple pathways, including the olfactory bulb, trigeminal nerve, and somatic circulation, with fluorescence intensity decreasing over time in all regions.[41] However, the nanoparticle-hydrogel group exhibited the slowest reduction in fluorescence intensity, indicating that the PueNps&Ac2-26 gel formulation had enhanced slow-release properties (Figure 2C).

## TTC Staining and Neurological Function Assessment

The animal experimental procedure is illustrated in (Figure 3A). Cerebral infarct volume in MCAO rats was assessed by TTC staining three days after intranasal administration (Figure 3B and C). The infarct volume in the model group was

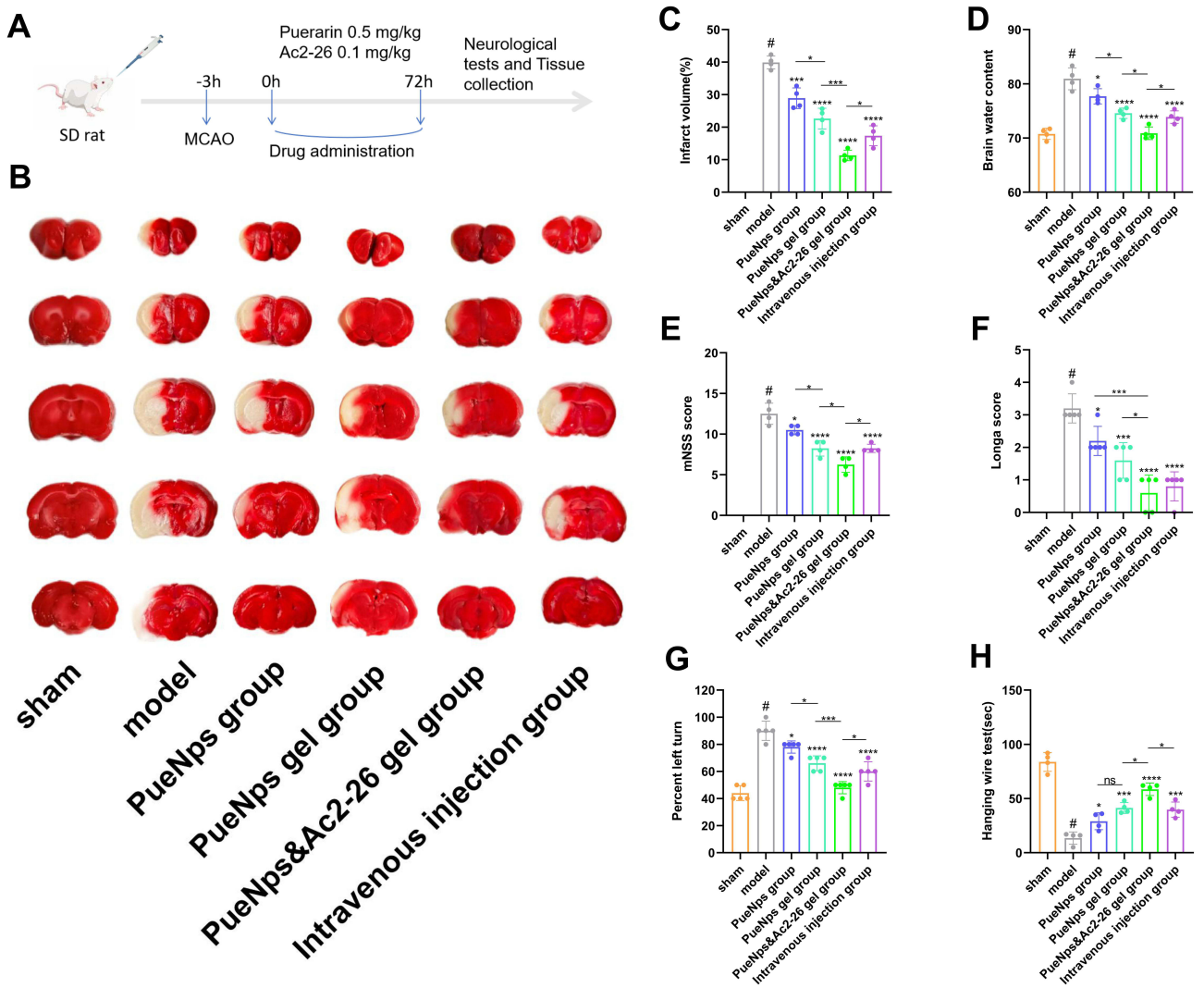


**Figure 3** In vivo assessment of treatment effects in different groups of rats. (**A**) Schematic diagram of the animal experiment procedure.(**B** and **C**) TTC staining to assess cerebral infarct volume (n=4). (**D**) Quantitative analysis of brain edema content (n=4). (**E**) mNSS neurologic function score (n=4). (**F**) longa score (n=5). (**G**) Cornering test experiment (n=5). (**H**) Wire hang test experiment (n=4). Data are expressed as mean ± standard deviation. #P < 0.05 for comparison with the sham-operated group, *P for comparison with the model group, *P < 0.05, ***P < 0.001, ****P< 0.0001, ns: not statistically significant.


https://doi.org/10.2147/IJN.S508800

significantly larger (39.91%) compared to the sham-operated group. Treatment with various formulations resulted in a reduction in cerebral infarct volume to 28.92%, 22.64%, 11.31%, and 17.36%, respectively. These results demonstrate that the intranasal PueNps&Ac2-26 gel group exhibited the most significant therapeutic effect in alleviating ischemic brain injury. Further assessment of cerebral edema revealed that all treatment groups effectively reduced brain edema. Notably, the intranasal PueNps&Ac2-26 gel group showed significantly better efficacy compared to the intravenous injection group ($P < 0.05$) (Figure 3D). To assess neurological function, we used the modified Neurological Severity Score (mNSS) and Longa score. The results showed that the intranasal PueNps&Ac2-26 gel group had significantly lower mNSS and Longa scores compared to the model group (Figure 3E and F). In the cornering test, the number of turns to the unimpaired side was significantly reduced in all treatment groups, with the PueNps&Ac2-26 gel group showing the most pronounced improvement (Figure 3G). Additionally, in the wire-hanging and balance beam tests (Figure 3H and Supplementary Figure S2A), the rats in the PueNps&Ac2-26 gel group exhibited significantly improved motor function, with longer retention times. Furthermore, rats in this group exhibited the least weight loss compared to the control group, with a slight upward trend in body weight (Supplementary Figure S2B).

## Molecular Docking

Molecular docking was employed to predict the binding interactions between puerarin, Ac2-26, and the cGAS-STING pathway. The docking results revealed strong hydrogen bonding and hydrophobic interactions between puerarin and both cGAS and STING proteins, along with electrostatic interactions between puerarin and cGAS. Ac2-26 also formed distinct hydrogen bonds with both cGAS and STING, indicating a strong interaction between the peptides and the cGAS-STING pathway, which may mediate the therapeutic effects observed in subsequent experiments (Supplementary Figure S3A–D).

## HE Staining

Histopathological analysis of the brain tissues revealed significant differences between the sham-operated and model groups. In the sham-operated group, the neuronal structure in the cerebral cortex was normal, with tightly arranged and intact neurons. In the model group, however, severe pathological changes were evident, including increased cell gaps, vacuole-like changes, neuronal nuclear solidification, and disintegration of Nissl bodies. Treatment with puerarin alone alleviated some of the edema and restored a small number of Nissl bodies, but the overall damage remained significant. However, supplementation with Ac2-26 greatly enhanced the therapeutic effect, significantly reducing edema, normalizing cell nuclei morphology, and increasing the presence of Nissl bodies, with neurons becoming more tightly arranged. These improvements were most pronounced in the intranasal administration group compared to the intravenous injection group (Figure 4).

## IHC

IHC analysis showed that the expression of cGAS and STING was significantly higher in the model group compared to the sham-operated group, as evidenced by the large number of yellow-brown granules (Figure 5A–D). Treatment with puerarin alone reduced the number of positive cells in the PueNps and PueNps gel groups. This effect was further enhanced in the PueNps&Ac2-26 gel group, which exhibited significantly lower expression of cGAS and STING compared to the intravenous injection group ($P < 0.05$).

## Western Blot

The results of Western blot (WB) were consistent with those of immunohistochemistry (IHC). Compared to the sham surgery group, the model group showed a significant increase in the expression of cGAS and STING, indicating activation of this signaling pathway. After treatment, the expression of cGAS and STING was inhibited, further supporting that our formulation exerts its effects by suppressing the cGAS-STING signaling pathway (Figure 5E).

## Enzyme-Linked Immunosorbent Assay (ELISA)

To further explore the anti-inflammatory effects of the formulations, we measured the levels of inflammation-related markers via ELISA. The model group exhibited significantly elevated levels of inflammatory cytokines compared to the

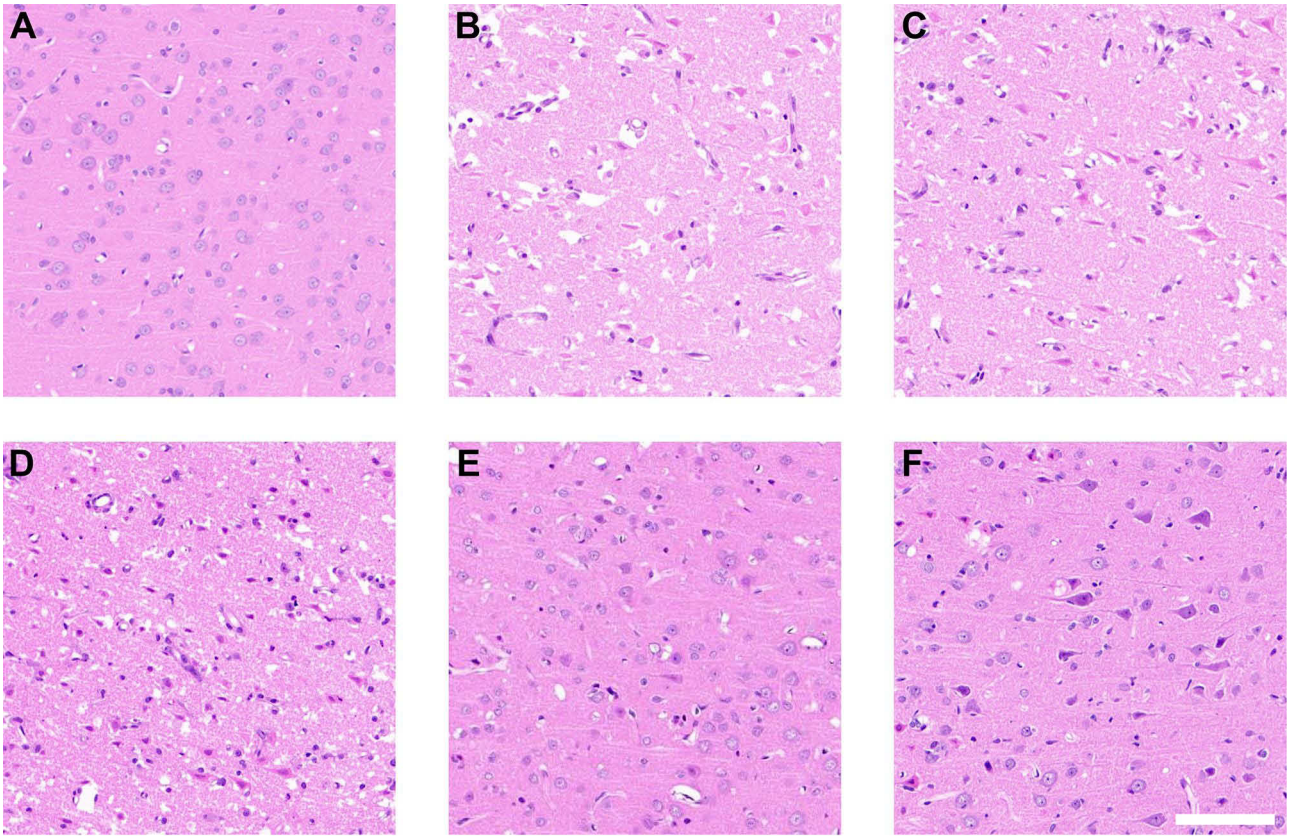


**Figure 4** HE staining of rat brain cortical tissues. (**A**) sham group; (**B**) model group; (**C**) PueNPs group; (**D**) PueNPs gel group; (**E**) PueNps&Ac2-26 gel group; (**F**) PueNps&Ac2-26 gel intravenous injection group. Scale bar = 100 um. (n=3).

sham-operated group, indicating a robust inflammatory response. Following treatment, all administration groups showed a marked decrease in inflammatory markers, with the PueNps&Ac2-26 gel group showing the most significant reduction compared to the puerarin-only treatment group (Figure 6A–C). Additionally, assays for oxidative stress markers revealed that, compared to the sham-operated group, the model group had significantly decreased levels of SOD and GSH and elevated levels of MDA, indicating oxidative stress. Treatment with the formulations led to increased levels of SOD and GSH, and a decrease in MDA levels, with the intranasal PueNps&Ac2-26 gel group demonstrating the most pronounced improvement (Figure 6D–F).

## In vitro Evaluation of Anti-Inflammatory Efficacy

As previously mentioned, following stroke, microglia are key players in neuroinflammation. They are rapidly activated and recruited to the ischemic brain region, where they release a large number of pro-inflammatory cytokines, exacerbating neuronal damage. Therefore, we utilized BV2 microglial cells to establish an OGD/R model to evaluate the in vitro anti-inflammatory effects of the different treatment groups. The results demonstrated that, compared to the control group, the OGD/R group exhibited significantly elevated levels of inflammatory factors. Both the PueNps and PueNps&Ac2-26 groups inhibited the expression of these inflammatory factors, with the PueNps&Ac2-26 group showing the most pronounced efficacy (Figure 7).

# Discussion

In recent years, researchers have focused on the development of alternative therapies for ischemic stroke to overcome the limitations of thrombolysis. Natural drugs, with their safety profiles, multi-targeted effects, and multifunctionality, have emerged as a promising area of research. Puerarin, a drug approved for clinical use by the Ministry of Health of China, is


https://doi.org/10.2147/IJN.S508800

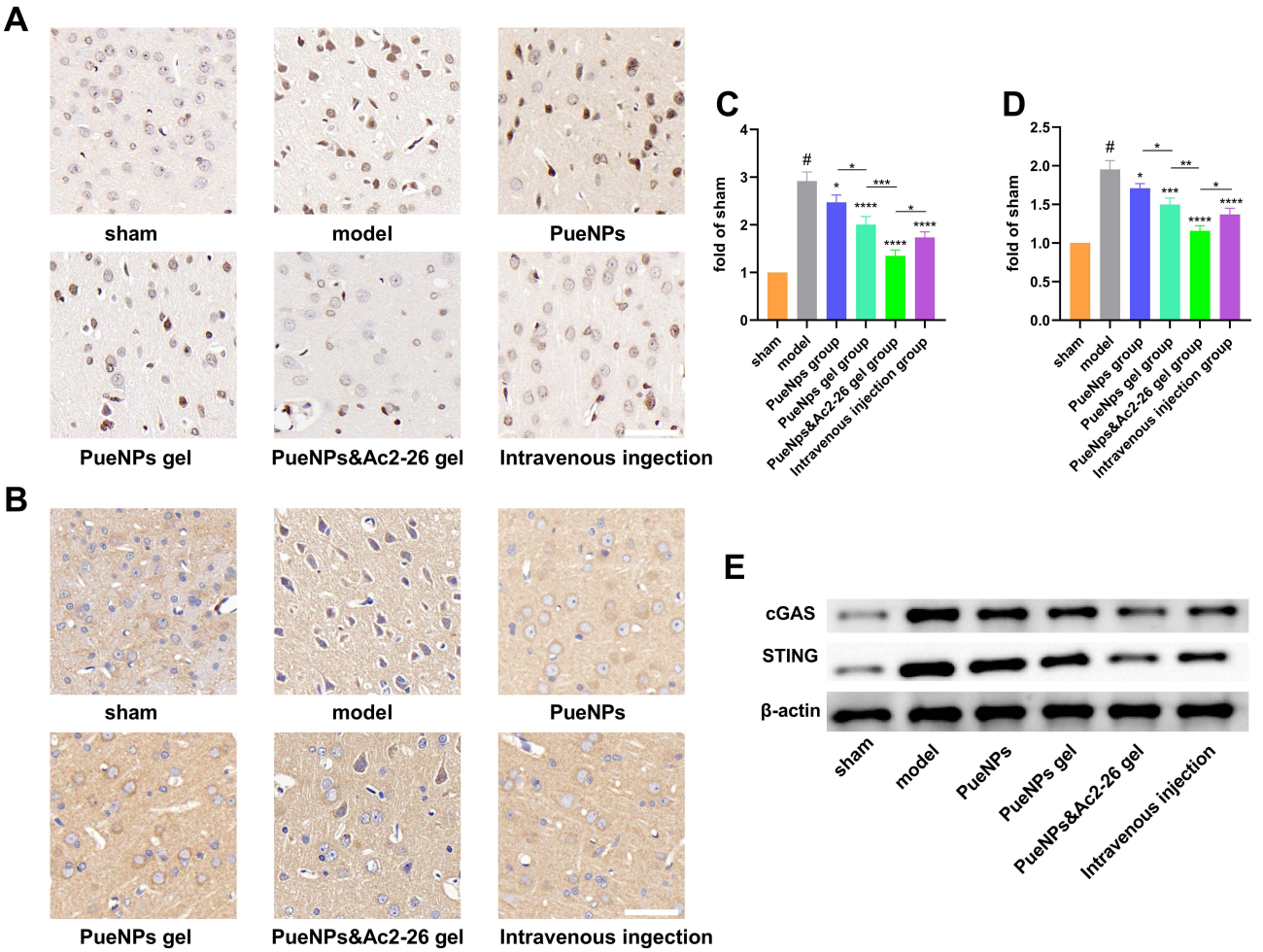


**Figure 5** IHC staining and quantitative analysis of cGAS and STING in rat brain. Scale bar = 50 um. (**A** and **C**) Representative images and quantitative analysis of cGAS protein expression in different treatment groups. (**B** and **D**) Representative images and quantitative analysis of STING protein expression in different treatment groups. (**E**) Western blot analysis of the expression levels of cGAS and STING proteins in rat brain tissue. Data are expressed as mean plus standard deviation (n=3). $^{\#}P < 0.05$ for comparison with the sham-operated group, *P for comparison with the model group, *P < 0.05, **P < 0.01, ***P < 0.001, ****P< 0.0001.

well-established in treating cardiovascular and cerebrovascular diseases due to its well-documented efficacy.[42] However, traditional drug combination strategies, often relying on two chemical agents, can increase the risk of side effects. In this study, we sought to avoid this by incorporating Ac2-26, a naturally occurring anti-inflammatory peptide. Ac2-26 is a beneficial compound in post-inflammation response responses, known for its lack of toxic side effects. Thus, this study aimed to design an optimal nanocarrier system to co-deliver puerarin and Ac2-26, enhancing the therapeutic potential in ischemic stroke treatment.

Among the various nanoparticle materials used in drug delivery, protein-based nanoparticles are especially notable for their specificity, biodegradability, low toxicity, and excellent biocompatibility. These characteristics make them an ideal choice for therapeutic delivery systems.[43] In our study, we successfully extracted bovine type I collagen using a combination of acid and enzyme methods. Collagen is a high-molecular-weight protein (Supplementary Figure S1A) with a unique triple-helix structure, which is resistant to common proteolytic enzymes and thus remains stable during delivery.[44] This structural stability is particularly crucial since the nasal cavity contains enzymes that could degrade the active substances of drug formulations.[45] Moreover, in intranasal drug delivery, nanoparticles must have an optimal particle size to ensure effective brain targeting. Usually, a particle size of less than 200 nm can effectively deliver therapeutic molecules to the brain.[46] Our particle size characterization results showed that the average particle size of the nanoparticles was approximately 132.92 nm, with a uniform particle size distribution, indicating that collagen

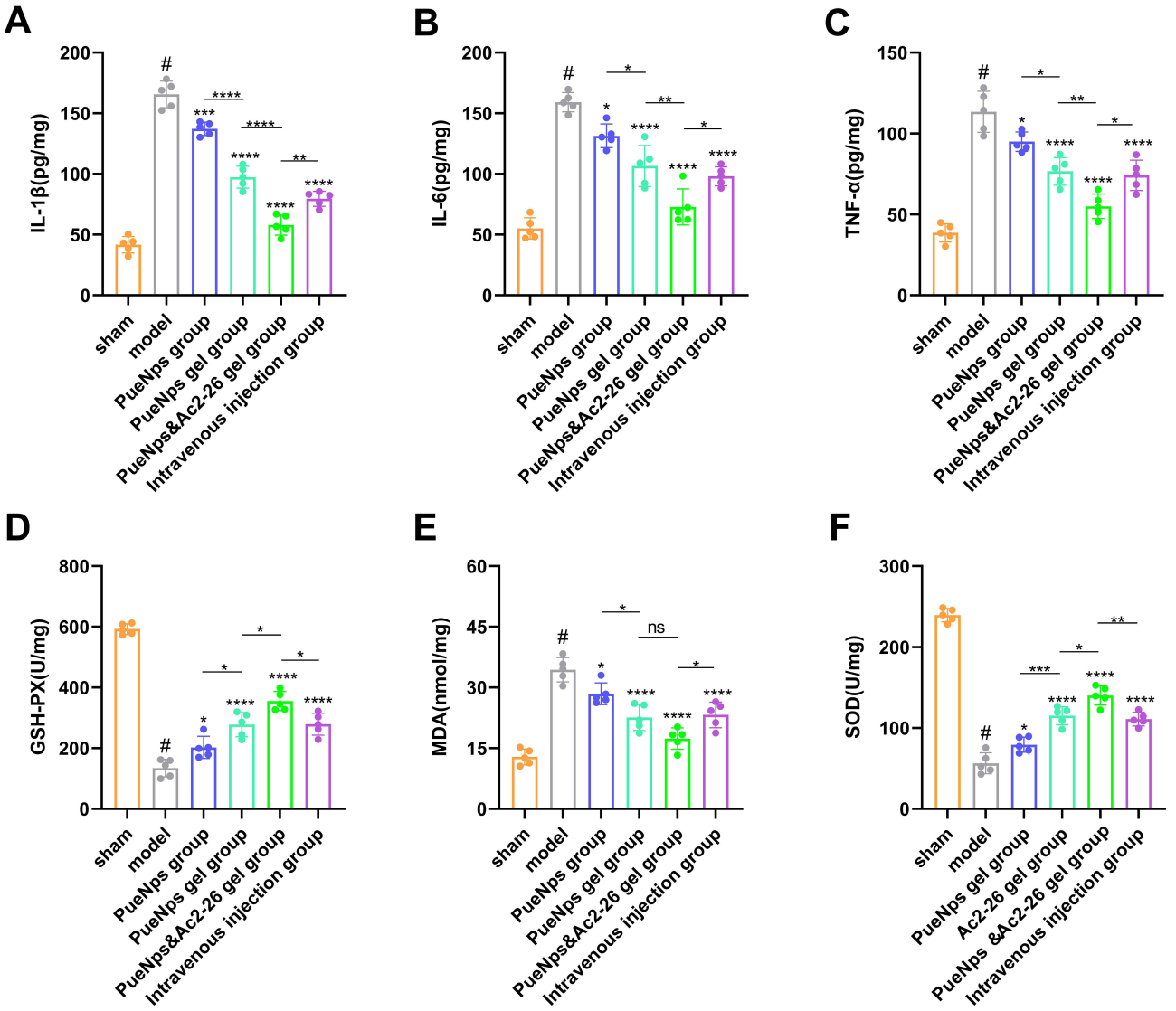


**Figure 6** Brain tissue inflammation and oxidative stress-related cytokine assays in different groups of rats after treatment. (**A–C**) Quantitative analysis of IL-1β, IL-6, and TNF-α inflammation-related cytokines, respectively. (**D–F**) Quantitative analysis of SOD, GSH-PX, and MDA oxidative stress-related cytokines, respectively. Data are expressed as mean plus standard deviation (n=5). #P < 0.05 for comparison with the sham-operated group, *P for comparison with the modeled group, *P < 0.05, **P < 0.01, ***P < 0.001, ****P< 0.0001, ns: not statistically significant.

nanoparticles with a smaller particle size were successfully prepared, making them very suitable for nasal drug delivery. In addition, surface charge also affects the stability of nanoparticles and their interaction with other biological interfaces.[47] In general, cationic nanoparticles possess higher cellular uptake rates than anionic nanoparticles, and although the surface potential is not necessarily a determining factor, at the same time, cationic nanoparticles also possess higher toxicity.[48,49] The collagen nanoparticles prepared by us possessed a high negative potential, which are not only safe but also do not aggregate between nanoparticles, ensuring their safe and efficient delivery.

Building upon this, we developed a hydrogel system that encapsulated both Ac2-26 and PueNps. The decision to incorporate a hydrogel was based on several considerations: firstly, to overcome the drawbacks of frequent administration of the biotherapeutic agent Ac2-26; secondly, to integrate two different therapeutic molecules into a single platform; thirdly, not to additionally increase the particle size of the nanoparticles, especially in intranasal delivery, where particle size affects delivery efficiency; and fourth, the hydrogel helps overcome some obstacles in the nasal cavity. For these reasons, we constructed an intranasal in situ hydrogel system and selected chitosan as the hydrogel matrix. Chitosan is obtained by alkaline deacetylation of naturally occurring chitin, which has excellent biocompatibility and


https://doi.org/10.2147/IJN.S508800

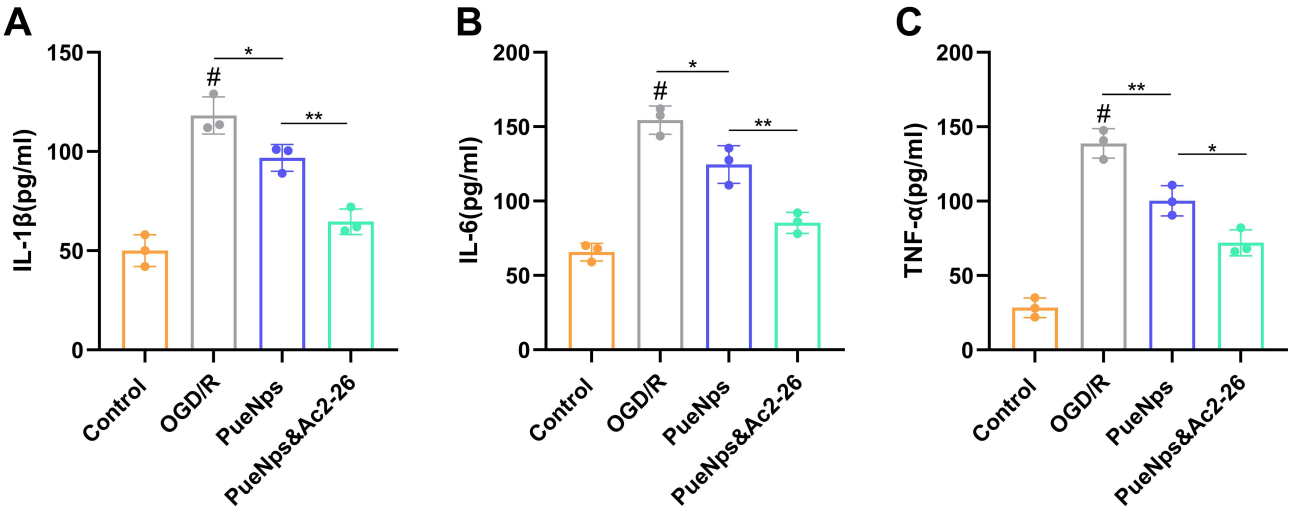


**Figure 7** In vitro evaluation of anti-inflammatory efficacy. (**A–C**) Quantitative analysis of IL-1β, IL-6, and TNF-α inflammation-related cytokines, respectively. Data are expressed as mean plus standard deviation (n=3). $^{\#}P < 0.05$ for comparison with the Control group, $^{*}P < 0.05$, $^{**}P < 0.01$.

biodegradability, is nontoxic, and is inexpensive and readily available.[50] In addition, chitosan can form a good adhesion with mucin through a variety of physical interactions, and this excellent adhesion improves delivery efficiency.[51] When the chitosan hydrogel is applied intranasally, the gel time and the gel temperature also affect the water gel's efficiency in prolonging the intranasal drug residence time.[6] In the present study, we prepared a hydrogel that, when administered intranasally, could rapidly form a gel within 3.3 minutes at physiologic nasal temperatures, which would help the hydrogel quickly adhere to the nasal mucosa, thereby reducing nasal clearance of foreign substances. This in situ gel formulation, which improves patient compliance, holds excellent potential for nasoencephalic drug delivery.[52] This suggest that the chitosan in situ temperature-sensitive hydrogel we prepared is capable of effective intranasal delivery of Ac2-26 and PueNps.

Regarding drug release kinetics, slow-release formulations have the advantages of prolonging the drug action time, reducing the adverse effects caused by rapid drug absorption, and reducing the frequency of drug administration.[53] The slow release of the formulations may also influence the bioavailability and bioactivity of the drugs.[54] Therefore, slow-release formulations have become a hot topic for research. However, there is still a need to explore safer and more efficient sustained-release drug delivery systems in the future.[55] In this study, we constructed a purely natural formulation system, ensuring safety. The drug release profile showed that the collagen nanoparticles could release the drug slowly and continuously, likely due to the dense collagen fibers trapping the drug in the interstitial space. The release of puerarin was further delayed by the addition of hydrogel, likely due to physical interactions between puerarin and chitosan hydrogel, thus, some of the puerarin was released with the degradation of the hydrogel. The slow release of Ac2-26 from the chitosan hydrogel compared to the release of free Ac2-26 (Supplementary Figure S1C) is hypothesized to be due to specific functional groups on chitosan, which can bind to Ac2-26 and thus significantly retard its release. In the formulation distribution study, the nanoparticle hydrogel group possessed the highest delivery efficiency compared to the other groups. This indicates that geraniol can undergo excellent slow release due to the dual-blocking effect of nanoparticles and hydrogel. Although the delivery efficiency of the DIR hydrogel group was not the highest, meaning that the efficacy of the Ac2-26 protein peptides could not be most fully utilized, it was considered acceptable, as explained above, based on the rationale for constructing the hydrogels. Moreover, further supplementation of Ac2-26 propeptide will exert better anti-inflammatory efficacy.

Next, we evaluated the efficacy of the formulation in rats. Studies on modification of puerarin using nanocarriers for the treatment of ischemic stroke have been reported. For example, puerarin cubic crystal nanoparticles, puerarin liposomes, and puerarin polybutylcyanoacrylate nanoparticles can improve the bioavailability of puerarin in the treatment of ischemic

stroke.[56–58] In contrast, the results of our formulation system, which was assessed for its in vivo efficacy in rats, showed that the optimized puerarin (PueNps group, PueNps gel group) effectively alleviated brain damage and exerted significant neuroprotective effects in rats, which is consistent with previous reports. However, we further supplemented the formulation with the human endogenous anti-inflammatory peptide. This anti-inflammatory agent system, after intranasal delivery, demonstrated more prominent efficacy in reducing the volume of cerebral infarction, alleviating cerebral edema, and improving the neurological function and behavioral deficits of the rats in the PueNps&Ac2-26 gel group compared to the PueNps gel group, which was further validated by HE staining, yielding consistent results. Furthermore, pharmacological data demonstrate that intranasal administration outperforms intravenous injection, primarily because intranasal delivery allows for better accumulation of the drug in ischemic brain tissue, minimizes plasma exposure, and mitigates peripheral side effects.[59] Nanotechnology further enhances the stability of the drug by reducing degradation, increasing its solubility, and improving its delivery to the brain.[60,61] Therefore, we propose that this formulation system and administration route could serve as a promising strategy to improve the therapeutic efficacy of ischemic stroke. In addition, we have conducted preliminary investigations into the potential molecular mechanisms underlying its effects.

Neuroinflammation disrupts immune homeostasis and worsens brain tissue damage following ischemic stroke. In the penumbra of ischemic brain tissue, necrotic neurons release substantial quantities of DNA fragments, leading to abnormal accumulation of free DNA in the ischemic area. Microglia, the first immune cells activated after brain injury, ingest these free DNA fragments, activating cGAS and, subsequently, STING.[62,63] STING is expressed in microglia, and its activation drives microglia toward a pro-inflammatory phenotype, triggering an inflammatory response.[64] Thus, the cGAS-STING signaling pathway is closely linked to microglia. Previous research has demonstrated that Ac2-26 can polarize microglia into an anti-inflammatory phenotype, thereby alleviating neuronal apoptosis, and puerarin can reduce microglial activation.[65,66] While both compounds strongly regulate microglial function, no studies have yet shown whether Ac2-26 and puerarin exert anti-inflammatory effects by inhibiting the cGAS-STING pathway. To address this, we first employed molecular docking techniques to explore the interaction between Ac2-26, puerarin, and cGAS-STING. We then validated these findings through immunohistochemistry and Western blotting. Our results indicate that puerarin exerts anti-inflammatory effects by inhibiting the cGAS-STING pathway. Although we did not independently verify whether Ac2-26 also inhibits the cGAS-STING pathway, the addition of Ac2-26 enhanced this inhibitory effect compared to the puerarin-only treatment group, likely due to their combined anti-inflammatory properties. Inflammatory factor assays further confirm that this formulation exhibits strong anti-inflammatory effects and alleviates oxidative stress.

Although the current research demonstrates promising results, several limitations remain. First, the specificity of nanoparticle targeting of the Ac2-26 peptide and the long-term stability of Ac2-26 are challenging to maintain. Secondly, the animal studies employed a relatively short administration period, lacking both long-term efficacy evaluations and additional research at the cellular level, as well as more detailed investigations into the underlying molecular mechanisms. Finally, while the formulation is composed of entirely natural components, extended animal safety assessments and comprehensive clinical trials are necessary to establish the safety of this formulation for human use.

## Conclusion

In this study, we developed a completely natural drug delivery system (PueNps&Ac2-26) that, upon nasal administration, facilitates the entry of puerarin and Ac2-26 into the brain. This system effectively inhibits the neuroinflammatory response following ischemic stroke, exerting a neuroprotective effect. This formulation not only provides a reference for the combined use of other natural drugs but also offers a promising approach for the clinical treatment of ischemic stroke in the future.

## Funding

This research was supported by Science and Technology Department of Jilin Province (Grant No. 20210204016YY, YDZJ202501ZYTS688).

## Disclosure

The authors report no conflicts of interest in this work.

## References


1. Martin SS, Aday AW, Almarzooq ZI. et al. American Heart Association Council on Epidemiology and Prevention Statistics Committee and Stroke Statistics Subcommittee. 2024 heart disease and stroke statistics: a report of US and global data from the American heart association. *Circulation*. 2024;149(8):e347–e913. doi:10.1161/CIR.0000000000001209.
2. Hilkens NA, Casolla B, Leung TW, et al. Stroke. *Lancet Lond Engl*. 2024;403(10446):2820–2836. doi:10.1016/S0140-6736(24)00642-1
3. Jurcau A, Simion A. Neuroinflammation in cerebral ischemia and ischemia/reperfusion injuries: from pathophysiology to therapeutic strategies. *Int J mol Sci*. 2021;23(1):14. doi:10.3390/ijms23010014
4. Wang Y, Yuan T, Lyu T, et al. Mechanism of inflammatory response and therapeutic effects of stem cells in ischemic stroke: current evidence and future perspectives. *Neural Regen Res*. 2025;20(1):67–81. doi:10.4103/1673-5374.393104
5. Gao M, Zhang Z, Lai K, et al. Puerarin: a protective drug against ischemia-reperfusion injury. *Front Pharmacol*. 2022;13:927611. doi:10.3389/fphar.2022.927611
6. Zhang Y, Zhang H, Zhao F, et al. Mitochond rial-targeted and ROS-responsive nanocarrier via nose-to-brain pathway for ischemic stroke treatment. *Acta Pharm Sin B*. 2023;13(12):5107–5120. doi:10.1016/j.apsb.2023.06.011
7. Wang D, Bu T, Li Y, et al. Pharmacological activity, pharmacokinetics, and clinical research progress of puerarin. *Antioxid Basel Switz*. 2022;11(11):2121. doi:10.3390/antiox11112121
8. Ucar B. Natural biomaterials in brain repair: a focus on collagen. *Neurochem Int*. 2021;146:105033. doi:10.1016/j.neuint.2021.105033
9. Zheng M, Wang X, Chen Y, et al. A review of recent progress on collagen-based biomaterials. *Adv Healthc Mater*. 2023;12(16):e2202042. doi:10.1002/adhm.202202042
10. Pires PC, Damiri F, Zare EN, et al. A review on natural biopolymers in external drug delivery systems for wound healing and atopic dermatitis. *Int J Biol Macromol*. 2024;263(Pt 1):130296. doi:10.1016/j.ijbiomac.2024.130296
11. Kurth M, Barayeu U, Gharibi H, et al. DOPA residues endow collagen with radical scavenging capacity. *Angew Chem Int Ed Engl*. 2023;62(24):e202216610. doi:10.1002/anie.202216610
12. Rathore P, Arora I, Rastogi S, et al. Collagen-curcumin nanocomposites showing an enhanced neuroprotective effect against short term focal cerebral ischemia. *RSC Adv*. 2020;10(4):2241–2253. doi:10.1039/c9ra08508d
13. Siddiqui MA, Asad M, Akhter J, et al. Resveratrol-loaded glutathione-coated collagen nanoparticles attenuate acute seizures by inhibiting HMGB1 and TLR-4 in the hippocampus of mice. *ACS Chem Neurosci*. 2022;13(8):1342–1354. doi:10.1021/acschemneuro.2c00171
14. Long Y, Yang Q, Xiang Y, et al. Nose to brain drug delivery - a promising strategy for active components from herbal medicine for treating cerebral ischemia reperfusion. *Pharmacol Res*. 2020;159:104795. doi:10.1016/j.phrs.2020.104795
15. Zha S, Liu H, Li H, et al. Functionalized nanomaterials capable of crossing the blood-brain barrier. *ACS Nano*. 2024;18(3):1820–1845. doi:10.1021/acsnano.3c10674
16. Ge Y, Xu X, Cao M, et al. Nasal drug delivery and nose-to-brain delivery technology development status and trend analysis: based on questionnaire survey and patent analysis. *Pharmaceutics*. 2024;16(7):929. doi:10.3390/pharmaceutics16070929
17. Fullerton JN, Gilroy DW. Resolution of inflammation: a new therapeutic frontier. *Nat Rev: Drug Discov*. 2016;15(8):551–567. doi:10.1038/nrd.2016.39
18. White ZB, Nair S, Bredel M. The role of annexins in central nervous system development and disease. *J Mol Med Berl Ger*. 2024;102(6):751–760. doi:10.1007/s00109-024-02443-7
19. Yuan J, Li L, Yang Q, et al. Targeted treatment of ischemic stroke by bioactive nanoparticle-derived reactive oxygen species responsive and inflammation-resolving nanotherapies. *ACS Nano*. 2021;15(10):16076–16094. doi:10.1021/acsnano.1c04753
20. Li C, Zhao Y, Cheng J, et al. A proresolving peptide nanotherapy for site-specific treatment of inflammatory bowel disease by regulating proinflammatory microenvironment and gut microbiota. *Adv Sci Weinh Baden-Wurtt Ger*. 2019;6(18):1900610. doi:10.1002/advs.201900610
21. Qin X, He L, Fan D, et al. Targeting the resolution pathway of inflammation using ac2-26 peptide-loaded pegylated lipid nanoparticles for the remission of rheumatoid arthritis. *Asian J Pharm Sci*. 2021;16(4):483–493. doi:10.1016/j.ajps.2021.03.001
22. Fredman G, Kamaly N, Spolitu S, et al. Targeted nanoparticles containing the proresolving peptide ac2-26 protect against advanced atherosclerosis in hypercholesterolemic mice. *Sci Transl Med*. 2015;7(275):275ra20. doi:10.1126/scitranslmed.aaa1065
23. Wang M, Ma X, Zong S, et al. The prescription design and key properties of nasal gel for CNS drug delivery: a review. *Eur J Pharm Sci*. 2024;192:106623. doi:10.1016/j.ejps.2023.106623
24. Perkušić M, Nodilo LN, Ugrina I, et al. Chitosan-based thermogelling system for nose-to-brain donepezil delivery: optimising formulation properties and nasal deposition profile. *Pharmaceutics*. 2023;15(6):1660. doi:10.3390/pharmaceutics15061660
25. Li T, Li S, Xiong Y, et al. Binary nano-inhalant formulation of icariin enhances cognitive function in vascular dementia via BDNF/TrkB signaling and anti-inflammatory effects. *Neurochem Res*. 2024;49(7):1720–1734. doi:10.1007/s11064-024-04129-5
26. Ojeda-Hernández DD, Velasco-Lozano S, Fraile JM, et al. Thermosensitive chitosan-based hydrogel: a vehicle for overcoming the limitations of nose-to-brain cell therapy. *Acta Biomater*. 2024;188:157–168. doi:10.1016/j.actbio.2024.09.002
27. Zhang M, Wu C, Lu D, Wang X, Shang G. cGAS-STING: mechanisms and therapeutic opportunities. *Sci China Life Sci*. 2025. doi:10.1007/s11427-024-2808-3
28. Li LJ, Liang SY, Sun XY, et al. Microglial double stranded DNA accumulation induced by DNase II deficiency drives neuroinflammation and neurodegeneration. *J Neuroinflammation*. 2025;22(1):11. doi:10.1186/s12974-025-03333-6
29. Zhang Z, Zhang C. Regulation of cGAS-STING signalling and its diversity of cellular outcomes. *Nat Rev Immunol*. 2025. doi:10.1038/s41577-024-01112-7
30. Zhang Y, Zou M, Wu H, Zhu J, Jin T. The cGAS-STING pathway drives neuroinflammation and neurodegeneration via cellular and molecular mechanisms in neurodegenerative diseases. *Neurobiol Dis*. 2024;202:106710. doi:10.1016/j.nbd.2024.106710
31. Sui H, Sun Z, Liu C, Xi H. Ferritinophagy promotes microglia ferroptosis to aggravate neuroinflammation induced by cerebral ischemia-reperfusion injury via activation of the cGAS-STING signaling pathway. *Neurochem Int*. 2025;183:105920. doi:10.1016/j.neuint.2024.105920
32. Maimaiti M, Li C, Cheng M, et al. Blocking cGAS-STING pathway promotes post-stroke functional recovery in an extended treatment window via facilitating remyelination. *Med N Y N*. 2024;5(6):622–644.e8. doi:10.1016/j.medj.2024.03.018

33. Liu M, Li Y, Han S, Wang H, Li J. Activin A alleviates neuronal injury through inhibiting cGAS-STING-mediated autophagy in mice with ischemic stroke. *J Cereb Blood Flow Metab off J Int Soc Cereb Blood Flow Metab*. 2023;43(5):736–748. doi:10.1177/0271678X221147056
34. Lv J, Zhu X, Xing C, et al. Stimulator of interferon genes (STING): key therapeutic targets in ischemia/reperfusion injury. *Biomed Pharmacother Biomedecine Pharmacother*. 2023;167:115458. doi:10.1016/j.biopha.2023.115458
35. Chauhan C, Kaundal RK. Understanding the role of cGAS-STING signaling in ischemic stroke: a new avenue for drug discovery. *Expert Opin Drug Discov*. 2023;18(10):1133–1149. doi:10.1080/17460441.2023.2244409
36. Siddiqui MA, Akhter J, Null A, et al. Resveratrol loaded nanoparticles attenuate cognitive impairment and inflammatory markers in ptz-induced kindled mice. *Int Immunopharmacol*. 2021;101(Pt A):108287. doi:10.1016/j.intimp.2021.108287
37. Li Y, Chen J, Quan X, et al. Extracellular vesicles maintain blood-brain barrier integrity by the suppression of caveolin-1/CD147/VEGFR2/MMP pathway after ischemic stroke. *Int J Nanomed*. 2024;19:1451–1467. doi:10.2147/IJN.S444009
38. Kang C, Sang Q, Liu D, et al. Polyphyllin I alleviates neuroinflammation after cerebral ischemia-reperfusion injury via facilitating autophagy-mediated M2 microglial polarization. *Mol Med*. 2024;30(1):59. doi:10.1186/s10020-024-00828-5
39. Yang Y, Wu Q, Shan X, et al. Ginkgolide B Attenuates Cerebral Ischemia-Reperfusion Injury via Inhibition of Ferroptosis through Disrupting NCOA4-FTH1 Interaction. *J Ethnopharmacol*. 2024;318(Pt B):116982. doi:10.1016/j.jep.2023.116982
40. CanKaraca A, Rezaei A, Qamar M, et al. Lipid-based nanodelivery systems of curcumin: recent advances, approaches, and applications. *Food Chem*. 2025;463:141193. doi:10.1016/j.foodchem.2024.141193
41. Botan MVG, Da silva JB, Bruschi ML. Technological strategies applied to pharmaceutical systems for intranasal administration of drugs intended for neurological treatments: a review. *AAPS Pharm Sci Tech*. 2024;25(8):258. doi:10.1208/s12249-024-02974-9
42. Wan Q, Lu Q, Luo S, et al. The beneficial health effects of puerarin in the treatment of cardiovascular diseases: from mechanisms to therapeutics. *Naunyn Schmiedebergs Arch Pharmacol*. 2024;397(10):7273–7296. doi:10.1007/s00210-024-03142-3
43. Kaltbeitzel J, Wich PR. Protein-based nanoparticles: from drug delivery to imaging, nanocatalysis and protein therapy. *Angew Chem Int Ed Engl*. 2023;62(44):e202216097. doi:10.1002/anie.202216097
44. Laronha H, Caldeira J. Structure and function of human matrix metalloproteinases. *Cells*. 2020;9(5):1076. doi:10.3390/cells9051076
45. Patharapankal EJ, Ajiboye AL, Mattern C, et al. Nose-to-Brain (N2B) delivery: an alternative route for the delivery of biologics in the management and treatment of central nervous system disorders. *Pharmaceutics*. 2023;16(1):66. doi:10.3390/pharmaceutics16010066
46. Butola M, Nainwal N. Non-invasive techniques of nose to brain delivery using nanoparticulate carriers: hopes and hurdles. *AAPS Pharm Sci Tech*. 2024;25(8):256. doi:10.1208/s12249-024-02946-z
47. Mura M, Carucci C, Caddeo E, et al. Specific buffer effects on the Formation of BSA protein corona around amino-functionalized mesoporous silica nanoparticles. *J Colloid Interface Sci*. 2025;677(Pt A):540–547. doi:10.1016/j.jcis.2024.07.258
48. Balog S, de Almeida MS, Taladriz-Blanco P, et al. Does the surface charge of the nanoparticles drive nanoparticle–cell membrane interactions? *Curr Opin Biotechnol*. 2024;87:103128. doi:10.1016/j.copbio.2024.103128
49. Ji Y, Wang Y, Wang X, et al. Beyond the promise: exploring the complex interactions of nanoparticles within biological systems. *J Hazard Mater*. 2024;468:133800. doi:10.1016/j.jhazmat.2024.133800
50. Geng Y, Xue H, Zhang Z, et al. Recent advances in carboxymethyl chitosan-based materials for biomedical applications. *Carbohydr Polym*. 2023;305:120555. doi:10.1016/j.carbpol.2023.120555
51. Lingait D, Rahagude R, Gaharwar S, et al. A review on versatile applications of biomaterial/polycationic chitosan: an insight into the structure-property relationship. *Int J Biol Macromol*. 2024;257(Pt 2):128676. doi:10.1016/j.ijbiomac.2023.128676
52. Garg A, Agrawal R, Singh Chauhan C, et al. In-situ gel: a smart carrier for drug delivery. *Int J Pharm*. 2024;652:123819. doi:10.1016/j.ijpharm.2024.123819
53. Andrade C. Sustained-release, extended-release, and other time-release formulations in neuropsychiatry. *J Clin Psychiatry*. 2015;76(8):20558. doi:10.4088/JCP.15f10219
54. Cai D, Wang X, Wang Q, et al. Controlled release characteristics of alkyl gallates and gallic acid from β-cyclodextrin inclusion complexes of alkyl gallates. *Food Chem*. 2024;460:140726. doi:10.1016/j.foodchem.2024.140726
55. Park K, Otte A, Li T. Bohemian rhapsody of future drug delivery systems: rational changes necessary for the next revolution. *Mol Pharm*. 2024;21(8):3732–3742. doi:10.1021/acs.molpharmaceut.4c00550
56. Chen J, Xu Y, Liu Y, et al. Preparation of cubic liquid crystal nanoparticles of puerarin and its protective effect on ischemic stroke. *Nanomedicine*. 2024;62:102786. doi:10.1016/j.nano.2024.102786
57. Luo C-F, Hou N, Tian J, et al. Metabolic profile of puerarin in rats after intragastric administration of puerarin solid lipid nanoparticles. *Int J Nanomed*. 2013;8:933–940. doi:10.2147/IJN.S39349
58. Zhao L, Liu A, Yu S, et al. The permeability of puerarin loaded poly(butylcyanoacrylate) nanoparticles coated with polysorbate 80 on the blood-brain barrier and its protective effect against cerebral ischemia/reperfusion injury. *Biol Pharm Bull*. 2013;36(8):1263–1270. doi:10.1248/bpb.b12-00769
59. Wang Z, Xiong G, Tsang WC, Schätzlein AG, Uchegbu IF. Nose-to-Brain Delivery. *J Pharmacol Exp Ther*. 2019;370(3):593–601. doi:10.1124/jpet.119.258152
60. Huang Q, Chen Y, Zhang W, et al. Nanotechnology for enhanced nose-to-brain drug delivery in treating neurological diseases. *J Control Release off J Control Release Soc*. 2024;366:519–534. doi:10.1016/j.jconrel.2023.12.054
61. Pires PC, Santos AO. Nanosystems in nose-to-brain drug delivery: a review of non-clinical brain targeting studies. *J Control Release*. 2018;270:89–100. doi:10.1016/j.jconrel.2017.11.047
62. Chauhan C, Kaundal RK. The role of cGAS-STING signaling in ischemic stroke: from immune response to therapeutic targeting. *Drug Discov Today*. 2023;28(11):103792. doi:10.1016/j.drudis.2023.103792
63. Ma X, Xin D, She R, et al. Novel Insight into cGAS-STING Pathway in Ischemic Stroke: from Pre- to Post-Disease. *Front Immunol*. 2023;14:1275408. doi:10.3389/fimmu.2023.1275408
64. Kong L, Li W, Chang E, et al. mtDNA-STING axis mediates microglial polarization via IRF3/NF-κB Signaling After Ischemic Stroke. *Front Immunol*. 2022;13:860977. doi:10.3389/fimmu.2022.860977
65. Xu X, Gao W, Li L, et al. Annexin A1 protects against cerebral ischemia-reperfusion injury by modulating microglia/macrophage polarization via FPR2/ALX-Dependent AMPK-mTOR Pathway. *J Neuroinflammation*. 2021;18(1):119. doi:10.1186/s12974-021-02174-3

66. Lim DW, Lee C, Kim I-H, et al. Anti-inflammatory effects of total isoflavones from pueraria lobata on cerebral ischemia in rats. *Molecules*. 2013;18 (9):10404. doi:10.3390/molecules180910404